J|A|C|S
JOURNAL OF THE AMERICAN CHEMICAL SOCIETY
Communication
pubs.acs.org/JACS

Morphology-Based Plasmonic Nanoparticle Sensors: Controlling Etching Kinetics with Target-Responsive Permeability Gate

Brian Malile and Jennifer I. L. Chen*

Department of Chemistry, York University, 4700 Keele Street, Toronto, Ontario Canada M3J 1P3

S Supporting Information

ABSTRACT: We present a sensing platform based on the morphological changes of plasmonic nanoparticles. Detection is achieved by using a stimulus-responsive polyelectrolyte-aptamer thin film to control the rate of diffusion of etchants that alter the shape and size of the nanoparticles. We show that the extent of morphological change and the colorimetric response depends on the amount of analyte bound. Contrary to conventional plasmonic sensors, our detection scheme does not rely on any interparticle interaction and is completely label-free, both in terms of the analyte and the capture probe. It presents new opportunities for designing facile, low-cost, and portable chip-based sensors for biodiagnostic and field analysis.

Rapid colorimetric detection without the need of sophisticated instrumentation is desirable for point-of-care biodiagnostic[1,2] and field detection. It enables preliminary on-site evaluation that can facilitate prognosis and decision-making in a timely manner with reduced cost. Many colorimetric sensors are based on colloidal stability of plasmonic nanoparticles in solutions[3−5] (e.g., aggregation or dissociation); however for reasons of portability and storage, substrate-based platforms (e.g., dip-sticks) are potentially more desirable and versatile. While nanoparticles can be readily anchored on a substrate, colorimetric chip sensors based on the conventional mechanism of nanoparticle aggregation may be ineffective because the majority (if not all) of the particles would be immobilized. Hence there is a need to explore new detection mechanisms that do not depend on the interaction between nanoparticles.

Plasmonic nanoparticles can exhibit highly tunable localized surface plasmon resonance (LSPR) in the visible wavelengths.[6,7] The energy of the plasmon can be tuned post-synthetically when the shape and size of the nanoparticle are altered, for example by chemical etchants such as halide ions.[8,9] The innate spectral sensitivity of LSPR to nanostructure morphology can provide the basis for versatile sensing platforms if changes in the nanostructure's shape or size can be induced upon analyte binding. Recent work related to morphology-based sensing explored the etching of gold nanorods[10] and silver nanoprisms;[11,12] however in all of the cases, the analyte had to take part in the etching process either by producing a chemical oxidant or by directly reacting with silver. This requirement could significantly limit the types of analytes that can be detected based on changes in the nanostructure morphology.

A more readily adaptable sensing platform based on spectral sensitivity to morphological changes would be one that decouples the roles of the analyte from the chemical echant. The analyte could enhance (or inhibit) the etching process, thus establishing a two-step sensing platform in which the sensor is first introduced to the sample and then analyzed chemically afterward. Herein we demonstrate the proof-of-concept and the generality of morphology-based colorimetric detection. We show that by incorporating an analyte-responsive polyelectrolyte thin film with plasmonic nanoparticles, the polyelectrolyte thin film acts as a gate to control the permeability of etchant molecules to the nanoparticles. The kinetics and extent of the morphological change depend on the presence or absence of the analyte, thereby yielding colorimetric differences that are discernible by eye.

Scheme 1 depicts our approach. The sensor consists of plasmonic nanoparticles anchored on a glass substrate and an overlayer of polyelectrolyte thin film on top of the nanoparticles. We use thin films from layer-by-layer assembly of polyelectrolytes containing DNA aptamers as a "biological gate" to control the diffusion of a chemical etchant. DNA aptamers are short oligonucleotides that can bind specifically to a wide range of analytes with high affinity.[13,14] We hypothesized that binding of analyte can increase the permeability of the polyelectrolyte thin film, as was suggested by others.[15] Hence a sample with analyte bound would see a greater change in the size or shape of the nanoparticle than the control when subsequently exposed to the etchant. A difference in the LSPR

Scheme 1. Morphology-Based Sensing Motif[a]

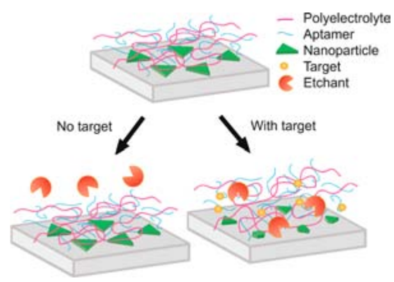

[a]Binding of target increases permeability and enhances etching of nanoparticles.

Received: August 20, 2013
Published: September 25, 2013

signal between the two films is observed by eye or detected with a spectrophotometer. For proof of principle, we use a fluorescent dye (sulforhodamine B) as the target because its aptamer has been isolated and its presence in the film can be monitored readily. Additionally we explore cocaine-binding aptamer for the detection of quinine to address the generality of this approach.

To fabricate the sensor, we synthesized gold-coated silver nanoprisms[16] (Ag@Au NP) and anchored them on a substrate via silanization with aminopropyltrimethoxysilane[17] (Figure S1). We chose silver nanoprisms because of their highly tunable LSPR.[18] By coating them with a thin layer of gold, they become stable in ionic solutions (e.g., NaCl) which are employed in the layer-by-layer polyelectrolyte deposition. We used polyallylamine hydrochloride (PAH) as the cationic polyelectrolyte and polystyrene sulfonate (PSS) and DNA aptamers as anionic polyelectrolytes. The layer-by-layer thin film is formed from the electrostatic interaction between PAH and the negatively charged nanoparticles and subsequently between oppositely charged polyelectrolytes. As the LSPR is sensitive to the refractive index, the layer buildup on the nanoparticles can be readily monitored by the peak shift in UV−vis spectra. Figure 1a shows the progression of the LSPR extinction spectra in air as more layers of PAH/PSS are assembled: bare Ag@Au NP film exhibits LSPR at 542 nm in air, and the peak red shifts linearly and then plateaus at 689 nm after eight bilayers. Figure 1b summarizes the shifts in LSPR peak for PAH/PSS vs PAH/DNA as a function of the number of bilayers on the Ag@Au NP. The smaller red shift for PAH/DNA than PAH/PSS can be attributed to different film thicknesses and the distance-dependence decay of LSPR.[19,20] The long PSS (MW ∼ 100 000 Da) can coil in ionic solutions[21] to forms thicker layers than DNA aptamer (MW = 9147 Da). Ellipsometry measurement confirms that a film of 10 bilayers of PAH/PSS is ∼38 nm thick, while that of PAH/DNA is only ∼18 nm. The refractive indices for the two films are comparable (1.43 vs 1.40 at 60% relative humidity).

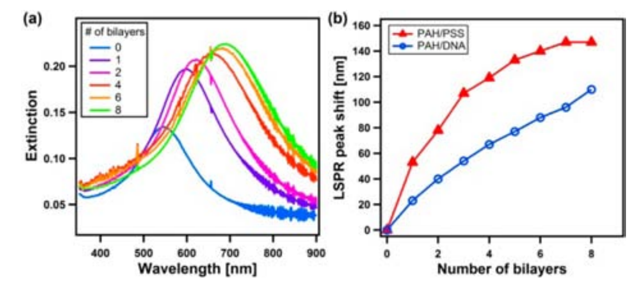

Figure 1. Monitoring layer-by-layer deposition via LSPR peak shift. (a) UV−vis spectra of the nanoparticle film on glass measured in air with increasing rounds of PAH/PSS deposition. (b) LSPR wavelength shift as a function of the number of bilayers of PAH/PSS (red triangles) vs PAH/DNA (blue open circles) deposited on the nanoparticle films.

We optimized the composition of the polyelectrolyte thin film for our sensing platform to be four bilayers of PAH/PSS followed by eight bilayers of PAH/DNA aptamer (denoted as $(PAH/PSS)_4(PAH/DNA)_8$ where the subscript refers to the number of bilayers). The $(PAH/PSS)_4$ base layer is required because the film of PAH/DNA deposited directly on top of nanoparticles was thin and possibly porous, making it challenging to elucidate the effect of analyte binding on permeability. Furthermore we find that more than four bilayers of PAH/DNA are needed to achieve analyte-binding induced permeability changes. The final $(PAH/PSS)_4(PAH/DNA)_8$ film has a thickness of ∼24 nm (at 60% relative humidity) as confirmed by ellipsometry.

Next we examine the binding affinity of the target sulforhodamine B to $(PAH/PSS)_4(PAH/DNA)_8$ assembled on Ag@Au NP by fluorescence spectroscopy. The binding affinity obtained from the Langmuir model gives K_d of 9.1 ± 1.9 μM in 1 mM KCl and 6.7 ± 2.2 μM in 0.1 M KCl (Figure S2a). These values are higher than aptamer in free solution[22] but close to previously reported value for polyelectrolyte-aptamer film.[23] The confocal fluorescence image (Figure S2b) of the polyelectrolyte-aptamer-nanoparticle film with dye bound shows good uniformity without cracks or large pores. The high fluorescence intensity confirms the aptamer's activity while embedded between PAH layers on top of the nanoparticles.

Our sensing platform requires a suitable chemical developer such as an etchant. Of the various compounds and compositions we explored, the mixture of 1 mM tetramethylammonium iodide and 0.01 mM I_2 is the most effective. We incorporated I_2 because iodide alone yields slow etching kinetics and reacts to form a passivating layer (AgI) on the nanoparticle surface. Furthermore, we hypothesized that the large tetramethylammonium[24] cation may enhance the effect of diffusion-controlled or site-hopping transport of the etchant. The resultant I^- and I_3^- ions in the mixture are effective for etching both gold and silver,[25] and their concentrations were optimized for our sensing platform (see Figure S3).

We now investigate the etching kinetics. Figure 2 shows the typical evolution of the UV−vis spectra of a Ag@AuNP/$(PAH/PSS)_4(PAH/DNA)_8$ film at different time intervals of etching. Initially the LSPR red shifts slightly and its intensity decreases. We obtain quantitative kinetics analysis by integrating the area under the spectra to approximate the number of atoms/electrons giving rise to LSPR.[9,26] Figure 2b

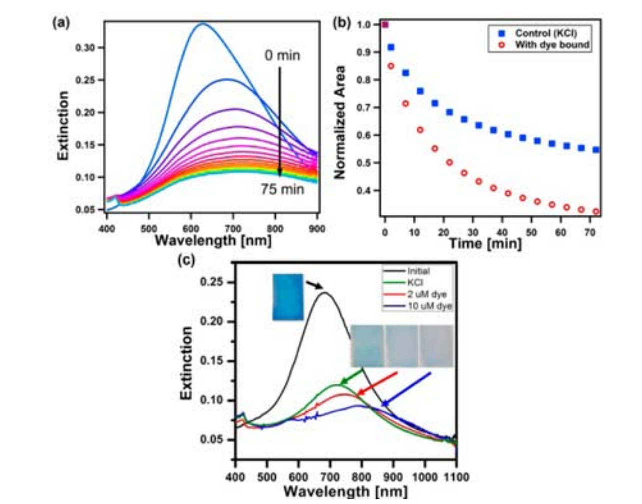

Figure 2. (a) Evolution of UV−vis spectra of a typical nanoparticle-polyelecrolyte-aptamer film during etching by I^-/I_3^- over 75 min. (b) Normalized integrated area of UV−vis spectra as a function of etching time for films pre-exposed to 0.1 M KCl (blue squares) or 10 μM dye at 0.1 M KCl (red open circles). (c) Dried film spectra before (black) and after etching for samples pre-exposed to 0.1 M KCl (green), 2 μM dye at 0.1 M KCl (red), and 10 μM dye at 0.1 M KCl (blue). The photographs of the corresponding films are shown in the inset.

shows the normalized area as a function of etching time for films with or without target bound: A faster initial decay and an overall greater extent of etching are observed for the film with sulforhodamine B bound (see Figure S4 and Table S1 for complete fitting analysis and statistics). Importantly, the polyelectrolyte overlayer remains intact, and the dye remains bound during the entire etching process (Figure S5). Figure 2c shows the dry spectra before and after etching along with photographs of the films pre-exposed to different concentrations of dye. The film that was immersed in 10 μM of dye exhibits the most pronounced red shift and the largest decrease in intensity. The final LSPR for film pre-exposed to 10 μM dye is centered at 805 nm with an extinction of 0.092, compared to the control film with LSPR at 721 nm and extinction of 0.12. Depending on the extent of etching, the color of the films varies from light blue to gray and is distinguishable visually. Moreover, we observed comparable etching kinetics even when an extra four bilayers of PAH/PSS was incorporated as capping layer on top of PAH/DNA (Figure S6). The facile iterative layer-by-layer methodology suggests the potential to incorporate other polyelectrolytes as the outermost layers to obtain nonfouling surfaces for reducing nonspecific interactions.[27,28]

The relative etching kinetics shown in Figure 2b suggests that the film with dye bound has a higher permeability to the I^-/I_3^- etchant and therefore an enhanced rate of morphological change of the nanoparticles. Several factors can influence the permeability of the polyelectrolyte film. First the sulforhodamine aptamer forms a G-quadruplex when the dye binds in the presence of K^+; this conformational change has been suggested to open up pores in the polyelectrolyte film as the PAH and DNA aptamer rearrange spatially.[15] Second, binding of the negatively charged dye can modify the intrinsic charge balance between PAH and DNA layers. This effect can lead to swelling or an increase in the permeability, as had been previously examined for acid/base polyelectrolytes films where ionic strengths or pH of the solution were changed.[29−31] To address the possibility of swelling due to a change in the electrostatic balance, we carried out ellipsometry at different relative humidity of polyelectrolyte films (in the absence of nanoparticles) with and without dye bound. Figure 3a shows a comparison of the thicknesses of the films (with or without dye) as a function of relative humidity. By increasing the relative humidity from 0 to 100%, the control film swells by 19%, while the film with dye swells by 28% of the original thickness. The swelling of the films is accompanied by a concomitant decrease in refractive index (Figure 3b) because water has a smaller refractive index (1.33) than the polyelectrolytes (1.42−1.55). The nominal increase in swelling when the dye is present may be attributed to changes in the electrostatic interaction. Additionally, it has been suggested that rearrangement of the polyelectrolyte can expose additional charged groups, thereby enhancing the site-to-site hopping of ions.[32] These factors are in line with our observation that dye-binding results in an enhanced rate of transport of the etchant ions and a faster etching of nanoparticles.

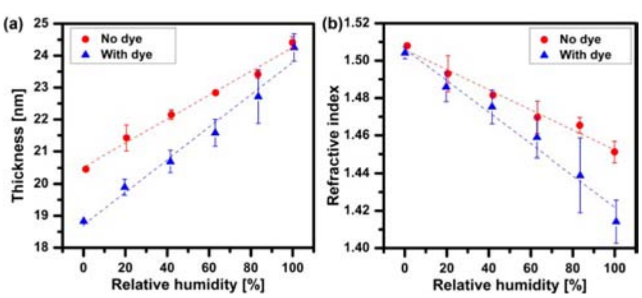

Figure 3. Ellipsometry measurements at different relative humidity for films ($(PAH/PSS)_4(PAH/DNA)_8$PDAC stamped on Si wafer) with or without dye bound. Plots of thickness (a) and refractive index (b) as a function of relative humidity. The data shown are averages obtained from the swelling and deswelling curves; dashed lines are linear fits (see Table S2). The film with dye bound shows a more significant swelling behavior.

If the conformational change of the aptamer upon target binding gives rise to a change in the permeability, then our sensing concept should be adaptable to other aptamers that fold into a secondary structure when the analyte binds. The charge of the analyte may be less important as electrostatic interaction seems to affect the swelling behavior marginally. We tested this hypothesis by exploring cocaine-binding aptamer in our sensor architecture. The aptamer is almost completely unstructured in the native state but forms three stems around a three-way junction[33] in the presence of cocaine or quinine[34] (Figure 4a).

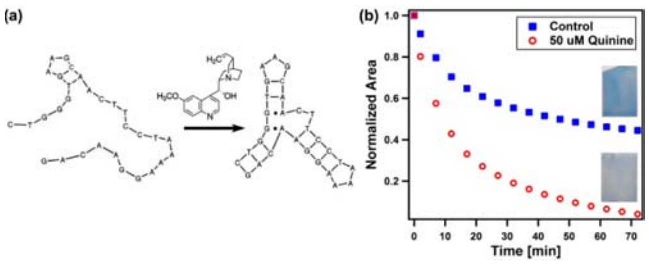

Figure 4. Sensing platform applied to the detection of quinine. (a) Schematic showing the conformational change of the cocaine-binding aptamer from unstructured state to three stems around a three-way junction upon binding to quinine. (b) Kinetics of etching for the control (blue squares) and sample pre-exposed to 50 μM of quinine (open red circles), obtained from the normalized integrated area of UV−vis spectra. Photographs of the etched films are shown in the inset.

Quinine is a weak base (K_b =9.6) that exists mostly in the neutral form for the concentrations investigated here. Figure 4b shows the etching kinetics of films with or without quinine bound; a significantly faster and more pronounced etching of the nanoparticles is observed when the film is pre-exposed to 50 μM of quinine. Additionally, we carried out control experiments to rule out the effects of analyte on the surface chemistry of bare nanoparticles and nonbinding interactions of the analyte that could influence the etching process (Figure S7). The results support the hypothesis that binding-induced changes in the polyelectrolyte layers ultimately facilitate the transport and diffusion of the etchant molecules.

In summary, we demonstrate a sensing platform based on the spectral sensitivity of plasmonic nanostructures to their morphology. We utilized thin films of polyelectrolyte-DNA aptamer as biological gate to control the diffusion of etchants that would alter the shape and size of plasmonic nanoparticles. This concept provides the basis for potentially low-cost, portable chip-based colorimetric sensors that are discernible by eye. Future work aims to explore the detection of other classes of analytes and to investigate the sensor's viability and performance in complex samples. Fundamental understanding of the aptamer's structure when embedded in the solid-state thin film would also be beneficial in elucidating the origin of the permeability change and for providing design rules for the biological probe. Moreover we envision that the colorimetric change can be improved by employing different types of plasmonic nanostructures and by finding a more effective chemical developer. When combined with consumer electronics (e.g., cell phone cameras) and simple optical filters, the sensing platform may enable facile and low-cost biodiagnostics that are critical in providing healthcare in developing countries, and offer dip-stick type sensors for use in field analysis for agriculture monitoring and environmental protection.

■ ASSOCIATED CONTENT

Supporting Information

Experimental details and additional data. This material is free of charge via the Internet at http://pubs.acs.org.

■ AUTHOR INFORMATION

Corresponding Author

jilchen@yorku.ca

Notes

The authors declare no competing financial interest.

■ ACKNOWLEDGMENTS

This work is supported by Natural Science and Engineering Research Council of Canada (NSERC) and a start-up fund from York University. We thank V. Kitaev and P. Johnson for helpful discussions, G. Ozin for instrument access, K. Rethoret for technical assistance, and J. Moir for ellipsometry measurements.

■ REFERENCES

(1) Giljohann, D. A.; Mirkin, C. A. *Nature* **2009**, *462*, 461.
(2) Rosi, N. L.; Mirkin, C. A. *Chem. Rev.* **2005**, *105*, 1547.
(3) Liu, J. W.; Lu, Y. *J. Am. Chem. Soc.* **2003**, *125*, 6642.
(4) Elghanian, R.; Storhoff, J. J.; Mucic, R. C.; Letsinger, R. L.; Mirkin, C. A. *Science* **1997**, *277*, 1078.
(5) Yan, Y.; Chen, J. I. L.; Ginger, D. S. *Nano Lett.* **2012**, *12*, 2530.
(6) Jin, R. C.; Cao, Y. W.; Mirkin, C. A.; Kelly, K. L.; Schatz, G. C.; Zheng, J. G. *Science* **2001**, *294*, 1901.
(7) Xiong, Y. J.; McLellan, J. M.; Chen, J. Y.; Yin, Y. D.; Li, Z. Y.; Xia, Y. N. *J. Am. Chem. Soc.* **2005**, *127*, 17118.
(8) Cathcart, N.; Frank, A. J.; Kitaev, V. *Chem. Commun.* **2009**, 7170.
(9) Espinoza, M. G.; Hinks, M. L.; Mendoza, A. M.; Pullman, D. P.; Peterson, K. I. *J. Phys. Chem. C* **2012**, *116*, 8305.
(10) Liu, X.; Zhang, S.; Tan, P.; Zhou, J.; Huang, Y.; Nie, Z.; Yao, S. *Chem. Commun.* **2013**, *49*, 1856.
(11) Chen, L.; Fu, X.; Lu, W.; Chen, L. *ACS Appl. Mater. Inter.* **2012**, *5*, 284.
(12) Jiang, X. C.; Yu, A. B. *Langmuir* **2008**, *24*, 4300.
(13) Osborne, S. E.; Ellington, A. D. *Chem. Rev.* **1997**, *97*, 349.
(14) Cho, E. J.; Lee, J.-W.; Ellington, A. D. *Annu. Rev. Anal. Chem.* **2009**, *2*, 241.
(15) Sultan, Y.; DeRosa, M. C. *Small* **2011**, *7*, 1219.
(16) Gao, C.; Lu, Z.; Liu, Y.; Zhang, Q.; Chi, M.; Cheng, Q.; Yin, Y. *Angew. Chem., Int. Ed.* **2012**, *51*, 5629.
(17) Can, X.; Zhi, L.; Mirkin, C. A. *Small* **2005**, *1*, 513.
(18) Metraux, G. S.; Mirkin, C. A. *Adv. Mater.* **2005**, *17*, 412.
(19) Whitney, A. V.; Elam, J. W.; Zou, S.; Zinovev, A. V.; Stair, P. C.; Schatz, G. C.; Van Duyne, R. P. *J. Phys. Chem. B* **2005**, *109*, 20522.
(20) Haes, A. J.; Zou, S.; Schatz, G. C.; Van Duyne, R. P. *J. Phys. Chem. B* **2003**, *108*, 109.
(21) Dobrynin, A. V.; Rubinstein, M. *Prog. Polym. Sci.* **2005**, *30*, 1049.
(22) Wilson, C.; Szostak, J. W. *Chem. Biol.* **1998**, *5*, 609.
(23) Sultan, Y.; Walsh, R.; Monreal, C.; DeRosa, M. C. *Biomacromolecules* **2009**, *10*, 1149.
(24) *Electrolyte Solutions*, 2nd ed.; Robinson, R. A., Stokes, R. H., Eds.; Dover Publications: London, 1970.
(25) Bailey, J. M.; Ritchie, I. M. *Electrochim. Acta* **1977**, *22*, 35.
(26) Mulvaney, P. *Langmuir* **1996**, *12*, 788.
(27) Ba, C.; Ladner, D. A.; Economy, J. *J. Membr. Sci.* **2010**, *347*, 250.
(28) Boudou, T.; Crouzier, T.; Ren, K.; Blin, G.; Picart, C. *Adv. Mater.* **2010**, *22*, 441.
(29) Hiller, J. A.; Rubner, M. F. *Macromolecules* **2003**, *36*, 4078.
(30) Kim, B.-S.; Vinogradova, O. I. *J. Phys. Chem. B* **2004**, *108*, 8161.
(31) Antipov, A. A.; Sukhorukov, G. B.; Mohwald, H. *Langmuir* **2003**, *19*, 2444.
(32) Farhat, T. R.; Schlenoff, J. B. *Langmuir* **2001**, *17*, 1184.
(33) Neves, M. A. D.; Reinstein, O.; Johnson, P. E. *Biochemistry* **2010**, *49*, 8478.
(34) Pei, R.; Shen, A.; Olah, M. J.; Stefanovic, D.; Worgall, T.; Stojanovic, M. N. *Chem. Commun.* **2009**, 3193.